

Band structure of the magnetic fcc pseudomorphs: Ni(100), Co(100), and Fe(100)

G. J. Mankey and R. F. Willis*

Department of Physics, The Pennsylvania State University, University Park, Pennsylvania 16802

F. J. Himpsel

IBM Thomas J. Watson Research Center, P.O. Box 218, Yorktown Heights, New York 10598

(Received 31 March 1993)

We report angle-resolved inverse-photoemission spectroscopy and ultraviolet-photoemission-spectroscopy measurements of the electronic structure of Cu(100), Ni(100), and pseudomorphic films of fcc Co and Fe on Cu(100). The unoccupied critical points at X are determined. These results are combined with recent photoemission data for use as input to an empirical combined-interpolation-scheme calculation of the energy-band dispersions for the allowed bands at $k^{\parallel}=0$. The ferromagnetic exchange splittings of the Δ_5 -symmetry $3d$ bands are estimated to be $\Delta E_{\text{ex}}=0.3$ eV, 1.2 eV, and 1.2 eV for Ni(100), Co(100), and Fe(100), respectively. The exchange splitting of the fcc Fe indicates that films deposited at room temperature are in the predicted low-spin magnetic phase. Annealing the Fe films produces a paramagnetic phase that exhibits no exchange splitting.

I. INTRODUCTION

The metastable fcc phases of the ferromagnets Co and Fe have attracted substantial interest, extending from fundamental aspects of metastable phases to possible applications in the magnetoresistive readout of magnetically stored information. Cobalt grows epitaxially in the fcc phase on Cu(100). Magnetic measurements of fcc Co films on Cu(100) have shown that the films have a thickness-dependent Curie temperature that varies according to film growth conditions.¹ Metastable fcc Fe can be stabilized epitaxially on Cu(100) or as inclusions in bulk Cu. It exhibits a very rich magnetic phase diagram, with small differences in strain stabilizing either an anti-ferromagnetic, a low-spin ferromagnetic, or a high-spin ferromagnetic phase. While the most stable phase appears to be the antiferromagnetic one found in Fe inclusions in a Cu matrix, and possibly for epitaxial Fe/Cu(100) after annealing to 500 K, there exists a higher total energy ferromagnetic phase on Cu(100) which is produced by room-temperature deposition up to a critical thickness of 12 monolayer (ML).^{2,3} Both fcc Fe and Co on Cu(100) display oscillatory magnetic coupling and giant magnetoresistance in multilayer structures.⁴ In fact, Co/Cu(100) is one of the most studied magnetic multilayer systems⁵⁻⁸ that exhibits one of the largest magnetoresistance effects, making it a prime test material for magnetoresistive readout systems.

The magnetic properties of metastable fcc Co and Fe films have been extensively investigated, but details of their underlying band structures are much less known. While there have been a number of publications dealing with various aspects of the band structure of any one of these materials, the aim of this work is to obtain a detailed comparison of the band dispersions in all of these magnetic pseudomorphs. That is, we present inverse-photoemission results on unoccupied states, together with

a systematic study of the trends in the band structure starting with the known bands of bulk Cu(100) and Ni(100), which we compare and contrast with results for thick films of fcc Co(100) and Fe(100) on Cu(100). The bands are parametrized by an empirical combined interpolation scheme involving plane-wave s,p bands hybridized with tight-binding $3d$ bands. Regarding the s,p bands we find that the Fermi level E_F moves up by 1 eV to 2 eV as the band filling increases in the transition metals Fe, Co, and Ni to the noble metal Cu (i.e., the critical points of the s,p bands at Γ and X move up relative to E_F in Cu). As a characteristic of the $3d$ bands we notice that the ferromagnetic exchange splitting of fcc Co on Cu(100) is similar to that of hcp Co, and that ferromagnetic fcc Fe on Cu(100) has only half the exchange splitting of bcc Fe, indicating a low-spin magnitude configuration.

Our focus here is on the epitaxial growth of metastable fcc phases of Co and Fe which are only stable in bulk form above 700 and 1183 K, respectively. Thin-film fcc phases can be formed on Cu(100) (see Refs. 1, 3, 9-12). They have also been observed as inclusions in bulk Cu.¹³ These epitaxial fcc phases are likely to be tetragonally distorted.¹⁴ Any residual misfit will induce a strain parallel to the surface, which gives rise to a strain of opposite sign perpendicular to the surface via the Poisson ratio. In addition, a weak surface reconstruction of the $n \times 1$ ($n \approx 5$) type is seen on the fcc Fe films grown at room temperature.^{15,16} In contrast to Co, for which total-energy calculations predict a stable ferromagnetic phase at the lattice constant of Cu,¹⁷ several magnetic phases of fcc Fe are predicted to occur at the lattice constant of Cu with nearly equal energy. Small distortions induced by strain or reconstruction may have a decisive effect on the magnetic behavior of Fe films. The most likely candidates are an antiferromagnetic phase and two ferromagnetic phases with high and low spin, according to local-density calculations.¹⁷⁻²² We observe that the

electronic structure of fcc Fe on Cu(100) exhibits at least two phases, a metastable room-temperature phase, and a more stable phase that is established after annealing above 500 K. These phases exist in temperature ranges concurrent with two magnetic phases that have been identified by a variety of magnetic techniques.^{23–32} Differences in their electronic band structure will be discussed in the following.

II. EXPERIMENT

The Cu(100) substrates were prepared using a procedure described previously.³³ For inverse-photoemission studies of Ni(100), a bulk Ni(100) crystal was prepared. An oxidation and reduction process was used to clean the Ni surface.³⁴ This crystal was superior in surface quality to another crystal prepared using the standard method of repeated sputter-anneal cycles, as evidenced by sharp image-potential surface states observed in the inverse-photoemission spectra. The pseudomorphic fcc Co(100) and Fe(100) films were grown at room temperature on Cu(100) substrates. The Co and Fe were sublimated from high-purity plates heated by electron bombardment. Typical evaporation rates were 0.5–1 Å/s.

Inverse-photoemission measurements were made in the constant-initial-state mode with a variable energy electron gun and grating spectrograph which has been described in detail elsewhere.³⁵ Photoemission measurements of the secondary electron distribution curves were made with a separate apparatus.³⁶ The sample was biased at -5.00 V for the photoemission measurements to minimize the effects of stray magnetic fields.

III. BAND DISPERSIONS

For inverse photoemission from the fcc(100) surface, only transitions from a free electronlike Δ_1 -symmetry band to bands with Δ_1 and Δ_5 symmetries are dipole allowed for normal incidence electrons. The Δ_1 band is s,p -like above the Fermi level and has a ferromagnetic ex-

change splitting of less than 0.1 eV which is not resolvable in our measurements. The Δ_5 band is d -like throughout the Brillouin zone, and only the minority-spin $\Delta_{5\downarrow}$ $3d$ band is observed in the inverse photoemission of ferromagnetic Ni(100) and Co(100). This greatly simplifies the interpretation of inverse-photoemission data since only two bulk bands are observable for normal incidence electrons.

By combining our own data of critical-point energies and Fermi-level crossings with recently published photoemission data, a set of critical points was evaluated and used as input for the quick fitting procedure of the combined-interpolation-scheme band-structure calculation described by Smith and Mattheiss.³⁷ The results are shown in Figs. 1(a)–1(e). Only two plane waves are used here, corresponding to the lower and upper Δ_1 -symmetry s,p band which hybridizes with the $3d$ band with like symmetry. This simplification is justified because the inclusion of a higher number of plane waves is necessary only to fit the band structure along the [100] direction far above E_F . Further, only the upper plane wave which propagates normal to the surface is involved in the photoemission process for normal emission or in the inverse-photoemission process for normal-incident electrons. The dispersions of the Δ_1 - and Δ_5 -symmetry minority-spin and majority-spin bands are calculated with the ferromagnetic exchange splitting of the $3d$ bands approximated as a constant, independent of k and E .

The band structure of Cu(100) is well known,³⁸ and the dispersions of both the occupied³⁹ and unoccupied states³³ have been measured. It will serve as a test of our empirical band-structure calculation. Ni(100) has been extensively studied, both with photoemission^{40,41} and inverse photoemission.^{42–44} Our measurements of the $X_{4'}$ and $X_{5\downarrow}$ critical-point energies complete the set of critical-point energies needed to parametrize the allowed bands along the ΓX direction. Co(100) layers on Cu(100) have been studied with spin-resolved photoemission.^{45–48} However, to our knowledge, there is no previously published work on the unoccupied electronic states for this

TABLE I. Critical-point energies for the fcc pseudomorphs. Majority-spin values are given for the spin-split $3d$ -like critical points. The s,p -like critical points have a splitting of less than 0.1 eV.

	Cu(100)	Ni(100)	Co(100)	Fe(100) (low spin)	Fe(100) (paramagnetic)
Γ_1	−8.6 ^a	−8.8 ^c	8.3 ^e	−8.0 ^g	−8.0 ^g
$\Gamma_{25'\uparrow}$	−3.56 ^a	−1.5 ^d	−2.2 ^f	−2.0 ^h	−1.0 ^g
$\Gamma_{12\uparrow}$	−2.75 ^a	−0.7 ^d	−1.0 ^f	−0.7 ^h	0.1
$X_{1\uparrow}$	−5.15 ^a	−3.6 ^d	−5.4 ^e	−4.6 ^h	−4.0
$X_{3\uparrow}$	−4.78 ^a	−3.1 ^c	−4.4 ^e	−4.0 ^h	−3.4
$X_{2\uparrow}$	−2.33 ^a	−0.3	−0.6 ^e	−0.2 ^h	0.6
$X_{5\uparrow}$	−2.03 ^a	−0.1 ^d	−0.4 ^f	0.1 ^h	0.9
$X_{4'}$	1.8 ^b	2.05	2.5	3.1	3.1
X_1	7.8	9.8	9.6	9.8	9.8
ΔE_{ex}	· · ·	0.3	1.2	1.2	· · ·
Φ	4.62	5.08	4.72	4.62	4.67

^aReference 38.

^bReference 33.

^cReference 41.

^dReference 40.

^eReference 59.

^fReference 47.

^gReference 49.

^hReference 22.

system. For Fe(100) layers on Cu(100), photoemission data have been published by several groups.^{49–51} The evolution of the unoccupied electronic states has recently been measured with inverse photoemission in the isochromat mode.⁵² These recent measurements show that bulklike electronic structure develops over the first few atomic layers.

The critical-point energies used for the fits are summarized in Table I. In most cases, the data points match the calculated values to within ± 0.2 eV. The experimental

data and the calculated bands for Cu(100) agree to within ± 0.1 eV, which is within our experimental resolution. For Ni(100) the spin-integrated photoemission data fall on the minority-spin band. This is expected since the half-width or lifetime of the transition increases linearly for transitions farther from the Fermi energy.^{53–55} Thus, the minority-spin transitions are sharper and more likely to be assigned to the observed peaks in the photoemission energy distribution curves. Our inverse-photoemission data determine the Fermi-level crossings of the Δ_1 and

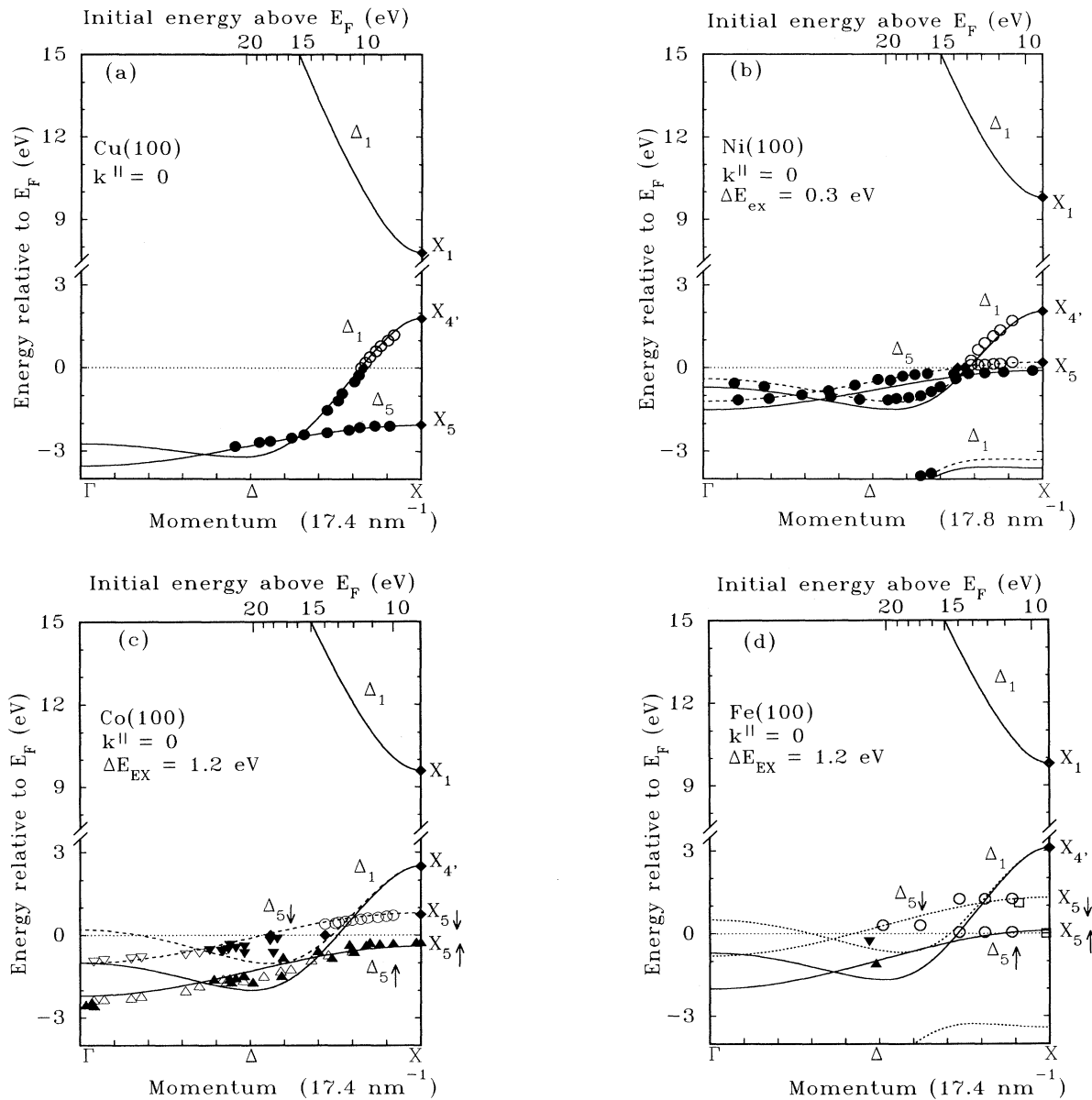


FIG. 1. Calculated band structure for the fcc pseudomorphs: Cu(100), Ni(100), Co(100), and Fe(100) along with inverse-photoemission data (open circles) from Fig. 5. Photoemission data for Cu and Ni are from Refs. 39 and 40. The plotted spin-polarized photoemission data for Co are from Ref. 47 (solid symbols) and Ref. 48 (open symbols). Upward pointing triangles signify majority spin and downward triangles indicate minority spin. Spin-polarized photoemission data for Fe are from Ref. 51 (solid triangles) and spin-integrated photoemission data are from Ref. 49 (solid circles). Inverse-photoemission data from Ref. 52 are plotted as open squares.

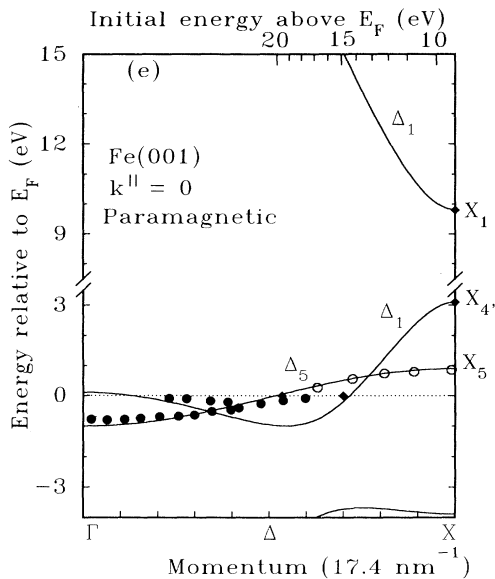


FIG. 1. (Continued).

$\Delta_{5\downarrow}$ bands and their dispersions in the vicinity of the X point.

For Co(100), the occupied majority-spin and minority-spin eigenvalues have been measured with spin-polarized photoemission and the spin polarizations are indicated by the up and down triangles, respectively.⁴⁶⁻⁴⁸ The exchange splitting for Co was taken to be 1.2 eV which is slightly less than the recently reported values of 1.4 ± 0.2 eV (Ref. 46) and 1.5 ± 0.15 eV.⁴⁸ The dispersion of the Δ_1 band cannot be determined from our inverse-photoemission measurements since the s,p states exhibit quantum-well resonances⁵⁶ which mask any emission from the Δ_1 states. The $\Delta_{5\downarrow}$ band shows up nicely in our measurements and its dispersion is accurately reproduced by the calculation.

For ferromagnetic Fe, the photoemission data are less complete, and the occupied critical-point energies for the calculation are taken from a recent self-consistent band-structure calculation.²² The occupied Fe critical-point energies in Table I were estimated by scaling the theoretical low-spin Fe values which overestimate the exchange splitting and the inner potential by a few tenths of an eV. The data for the $\Delta_{5\downarrow}$ band show less dispersion than the calculation. This effect could be due to only the topmost surface layers being ferromagnetic; recent surface magneto-optic Kerr-effect measurements have indicated that this is the case.¹⁵ These latter measurements¹⁵ imply that the film's electronic structure is actually a mixture of ferromagnetic low-spin Fe(100) for the topmost layers and paramagnetic Fe(100) for the underlying layers. A pure paramagnetic phase can be produced by annealing the film to 200°C. The annealing process produces films with a segregated layer of Cu on the surface. There is an associated change in the structure of the Fe when this occurs,¹⁴ and the atomic volume of the Fe is such that the paramagnetic phase is stable. The results are shown in Fig. 1(e). Also plotted is photoemission data taken from

a film in this metastable paramagnetic phase.⁴⁹

The experimental band dispersions can be used to test theoretical predictions¹⁷⁻²² of the magnetic structure of fcc Fe at the lattice constant of Cu. First we will discuss the metastable, room-temperature phase. Here we have to consider ferromagnetic phases only, since spin-polarized photoemission²³⁻²⁷ and other magnetic measurements²⁸⁻³² indicate ferromagnetic behavior. For ferromagnetic fcc Fe constrained to the lattice constant of Cu, there is the possibility of two phases which differ by a factor of 2 in the magnetic moment. The high-spin phase has a moment of $2.8\mu_B$, which is larger than the moment of $2.2\mu_B$ of the bcc phase at equilibrium. The low-spin phase which has a moment of approximately $1.4\mu_B$ exists only over a small range of atomic volume, corresponding to pseudomorphic films on Cu(001). This follows the expected decrease in the magnetic moment with a reduction in atomic volume, since fcc Fe has a 0.5% smaller volume at the lattice constant of Cu than the bcc phase at equilibrium. We expect to obtain meaningful clues to the electronic structure of fcc Fe by comparing theoretical and experimental band dispersions in Fig. 1. It is obvious that the calculated high-spin bands have a magnetic splitting too large to account for the data points, while the low-spin bands fit reasonably well. There are no inverse-photoemission features in the neighborhood of the high-spin $X_{5\downarrow}$ point. The observed Fermi-level crossing of the $\Delta_{5\downarrow}$ band near the middle of the Δ axis is also indicative of the low-spin band structure. Otherwise the crossing would be closer to Γ . A rigid shift of theoretical high-spin bands to accommodate the data is not possible since the density of the $3d$ states is so high near the Fermi level that the total number of electrons cannot be conserved. The calculated low-spin moment also fits the available magnetic measurements, which give at most $1.5\mu_B$, or even less when going to thicker films or annealing.²⁸ It is worthwhile to note that magnetic splitting and magnetic moment are nearly proportional to each other in the local-density calculations with a ratio of $0.92 \text{ eV}/\mu_B$ for the high-spin phase and $0.91 \text{ eV}/\mu_B$ for the low-spin phase. The approximate ratio of $1 \text{ eV}/\mu_B$ appears to be valid for an even wider class of magnetic systems which is discussed in more detail elsewhere.^{57,58}

IV. DETERMINATION OF CRITICAL POINTS AND FERMI-LEVEL CROSSINGS

The dispersion of the initial-state band must be established for the interpretation of photoemission and inverse-photoemission data. Thick (> 5 ML) bulklike films of Ni, Co, and Fe were prepared and the low-kinetic-energy secondary electron energy distribution curves were measured. The distributions reflect the one-dimensional densities of states of the final-state band in photoemission (initial-state band in inverse photoemission) along the surface normal. The inflection points in the spectra give the position of the Δ_1 final-band minimum below which only evanescent states or indirect transitions are observed. The results for Ni, Co, and Fe in Fig. 2 show the derivatives of the energy distribution curves which determine the inflection points in the spec-

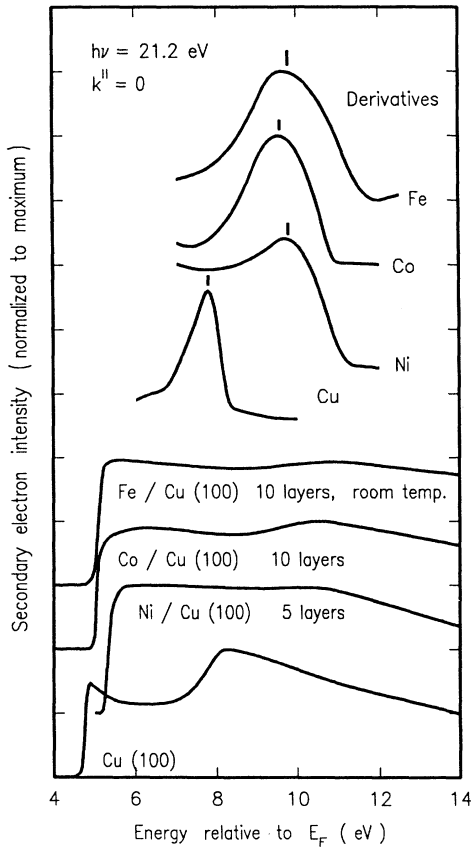


FIG. 2. Secondary electron energy distribution curves for Cu(100), Ni(100), Co(100), and Fe(100). The energies of the X_1 critical points are determined from the derivative spectra.

tra. The measured energies of the X_1 critical points are summarized in Table I.

The X_4' critical-point energy is determined from the cutoff in the inverse-photoemission spectrum taken at an initial energy high enough to avoid any direct transitions. A comparison of spectra from Cu(100) and Ni(100) is shown in Fig. 3. In the absence of direct transitions, these spectra are representative of the one-dimensional density of states along the $\Gamma\Delta X$ direction, and the energy of the X_4' point is taken as the energy where the derivative of the spectrum is a minimum. The energy of the X_4' point for Cu also corresponds to the asymptote of the $n = 1$ quantum-well state in the limit of large film thickness. The energy of the X_4' point for Co films on Cu was determined by this method, since Co films also exhibit quantum-well resonances. For the Fe films, we scaled the energy of the X_4' point of Cu up by the observed energy shift of the s,p band reported by Glatzel *et al.*⁵² for an eight-layer film.

Since the incident-electron energy can be varied continuously with the inverse-photoemission apparatus, the value of the perpendicular momentum probed can be continuously varied. By measuring the photoyield at the Fermi energy as a function of incident-electron energy,

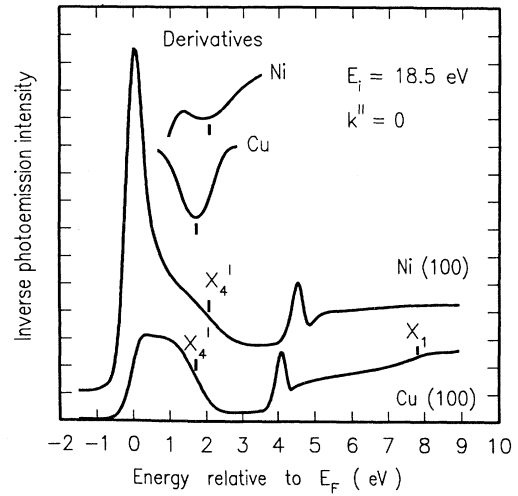


FIG. 3. Inverse-photoemission spectra of Cu(100) and Ni(100) at an initial energy high enough to avoid any bulk transitions. The spectra reflect the one-dimensional density of states along the surface normal and the X_4' critical-point energy is determined from the derivative spectra.

the Fermi energy crossings of the allowed bands can be determined. The Fermi-level crossings of the $\Delta_1 s,p$ bands and minority-spin $\Delta_{5\downarrow} 3d$ bands are seen as maxima in the inverse-photoemission intensity in Fig. 4. These crossings provide a check of the empirical band-structure calculations for which the energies agree to within a few

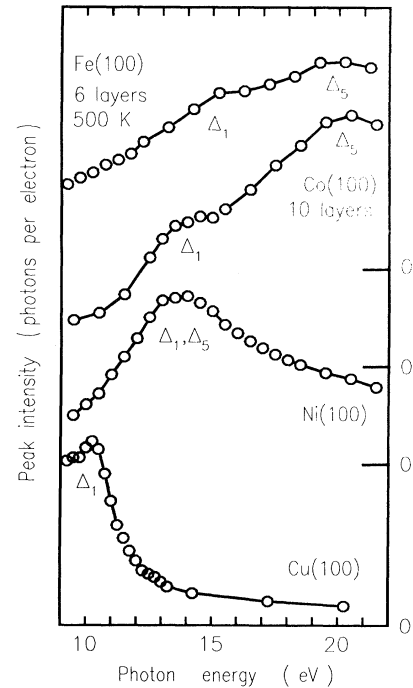


FIG. 4. Fermi-level intensity vs initial energy for Cu(100), Ni(100), and thick films of fcc Co(100) and Fe(100). The points where the energy bands cross E_F are seen as maxima in the intensity.

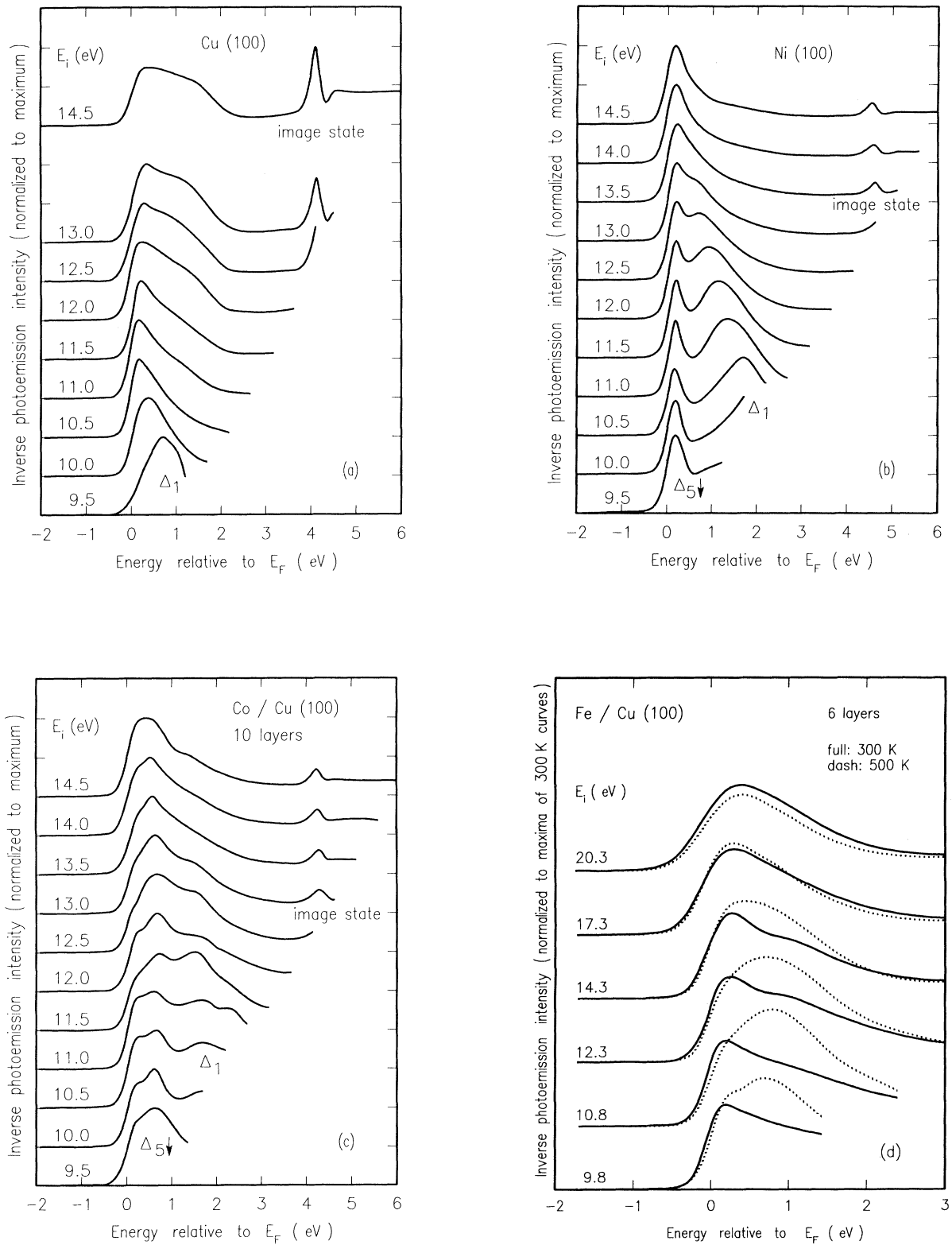


FIG. 5. Inverse-photoemission spectra for (a) Cu(100), (b) Ni(100), (c) thick films of Co, and (d) Fe on Cu(100) at varying initial electron energy E_i . The two transitions seen in the Ni spectra correspond to the minority-spin Δ_5 band and the Δ_1 band. For 10 ML Co/Cu(100), the Δ_1 band is chopped up into discrete quantum-well states due to the finite thickness of the film. For 6 ML Fe/Cu(100) the electron structure is different for as-deposited (solid lines) and annealed to 200 °C (dotted lines) films.

tenths of an eV. The Fermi-level crossing of the Δ_5 band for the Fe(100) film corresponds to the paramagnetic phase, which was produced by annealing the 6 ML Fe film to 200 °C.

V. INVERSE-PHOTOEMISSION MEASUREMENTS OF BAND DISPERSION

In order to assign the observed inverse-photoemission structures we have to consider the band topology and selection rules for the fcc surface along the [100] direction. The only allowed transitions for inverse photoemission with incident electrons normal to the surface are from a single Δ_1 upper band to one Δ_1 and one Δ_5 lower band, each split magnetically. Our photon detection geometry (unpolarized detection 45° from the surface normal) favors the Δ_5 band by a factor of 3, since it is associated with the component of the electric-field vector parallel to the surface, while the Δ_1 band is associated with the component of the electric-field vector perpendicular to the surface. The spectra for fcc Cu, Ni, Co, and Fe are shown in Figs. 5(a)–5(d).

For Cu(100), only the $\Delta_1 s,p$ band is seen since the 3*d* bands are far below E_F . It crosses the Fermi level at 10.5 eV, and spectra above this energy show a broad, featureless background due to indirect transitions. For Ni(100), the interpretation of the data is straightforward. The highly dispersive transition in Fig. 5(b) corresponds to the $\Delta_1 s,p$ band and the sharp transition that appears just above the Fermi energy in the spectra for incident-electron energies $E_i < 14$ eV is the minority-spin $\Delta_{5\downarrow}$ 3*d* band. For Co(100), more than two peaks are observed in the low-energy spectra, with the multiple peaks merging into a broad background at higher energies due to the degrading spectrometer resolution at higher initial electron energy E_i . The extra peaks are quantum-well states derived from the s,p band in thin films which have been discussed in detail elsewhere. The most intense feature in the spectra is the $\Delta_{5\downarrow}$ band which is unaffected by quantum size effects because the 3*d* electrons are more localized.

The Fe(100) data have no well-resolved features in the as-deposited spectra. The quantum-well states of the s,p band are smeared into a broad background due to film roughness and/or disorder. Although we cannot com-

pletely rule out the Δ_1 final band without observing it in the corresponding polarization geometry, there are several indications that the features in Fig. 5(d) are exclusively due to the Δ_5 band. The cross section for the analogous $\Delta_1 s,p$ band in Cu(100) [Fig. 5(a)] is small compared to the 3*d*-like Δ_5 band of fcc Fe(100) for initial energies above 12 eV. A similar cross section behavior is expected for the $\Delta_1 s,p$ band in fcc Fe. Even at low excitation energies, where the $\Delta_1 s,p$ band cross section is large, it can be distinguished from the Δ_5 band by its strong dispersion. We find much less dispersion with k_{\parallel} as well as k_{\perp} for the features in fcc Fe than for the Δ_1 transition of the Cu(100) substrate. The dashed lines show the effect of annealing the film. Some Cu surface segregation occurs upon annealing the film as is evidenced by the increase in intensity near the Fermi energy for the low-energy spectrum. The associated structural change of the film produces a paramagnetic phase of Fe(100) where the dispersion of the unpolarized Δ_5 band is revealed.

VI. SUMMARY

In summary, the unoccupied critical points and band dispersions of the magnetic fcc pseudomorphs Ni(100) and epitaxial films of Co(100) and Fe(100) on Cu(100) have been measured. The data were used together with published photoemission data as inputs to a combined-interpolation-scheme calculation of the dispersions for the allowed bands observed along the [100] direction. Ni and Co are both in stable ferromagnetic phases with measured exchange splittings of $\Delta E_{\text{ex}} = 0.3$ and 1.2 eV, respectively. Fe films on Cu(100) are both structurally and magnetically metastable. For room-temperature deposition, the bulklike Fe films exhibit an exchange splitting of $\Delta E_{\text{ex}} = 1.2$ eV. The Fe films irreversibly convert to a paramagnetic phase upon annealing to 200 °C.

ACKNOWLEDGMENTS

G.J.M. and R.F.W. wish to acknowledge funding from the National Science Foundation under Grant No. NSF-DMR 9121736, and a collaborative agreement with the IBM corporation.

*Author to whom correspondence should be sent.

¹J. J. de Miguel, A. Ceboladda, J. M. Gallego, R. Miranda, C. M. Schneider, P. Schuster, and J. Kirshner, *J. Magn. Magn. Mater.* **93**, 1 (1991).

²S. H. Lu, J. Quinn, D. Tian, and F. Jona, *Surf. Sci.* **209**, 364 (1989).

³M. T. Kief and W. F. Egelhoff, Jr., *Phys. Rev. B* **47**, 10 785 (1993).

⁴F. Petroff, A. Barthelemy, D. H. Mosca, D. K. Lottis, A. Fert, P. A. Schroeder, W. P. Pratt, Jr., R. Loloee, and S. Lequien, *Phys. Rev. B* **44**, 5355 (1991).

⁵B. Heinrich, J. F. Cochran, M. Kowalewski, J. Kirshner, Z.

Celinski, A. S. Arrott, and K. Myrtle, *Phys. Rev. B* **44**, 9348 (1991).

⁶M. T. Johnson, S. T. Purcell, N. W. E. McGee, R. Coehoorn, J. van de Stegge, and W. Hoving, *Phys. Rev. Lett.* **68**, 2688 (1992).

⁷Z. Q. Qui, J. Pearson, and S. D. Bader, *Phys. Rev. B* **46**, 8659 (1992).

⁸P. Bruno and C. Chappert, *Phys. Rev. Lett.* **67**, 1602 (1991); **67**, 2592 (1991).

⁹P. Dastoor, M. Arnott, E. M. McCash, and W. Allison, *Surf. Sci.* **272**, 154 (1992).

¹⁰S. Ferrer, E. Vlieg, and I. K. Robinson, *Surf. Sci.* **250**, L363

- (1991).
- ¹¹H. Glatzel, Th. Fauster, B. M. U. Scherzer, and V. Dose, *Surf. Sci.* **254**, 58 (1991).
 - ¹²D. A. Steigerwald and W. F. Egelhoff, Jr., *Surf. Sci.* **192**, L887 (1987).
 - ¹³C. L. Chen, S. H. Liou, D. Kofalt, Wu Yu, T. Egami, and T. R. McGuire, *Phys. Rev. B* **33**, 3247 (1986).
 - ¹⁴H. Magnan, D. Chandris, B. Villette, O. Heckmann, and J. Lecante, *Phys. Rev. Lett.* **67**, 859 (1991).
 - ¹⁵J. Thomassen, F. May, B. Feldman, M. Wuttig, and H. Ibach, *Phys. Rev. Lett.* **69**, 3831 (1992).
 - ¹⁶W. Daum, H. Stuhlmann, and H. Ibach, *Phys. Rev. Lett.* **60**, 2741 (1988).
 - ¹⁷V. L. Moruzzi, P. M. Marcus, K. Schwarz, and P. Mohn, *Phys. Rev. B* **34**, 1784 (1986).
 - ¹⁸Genrich L. Krasko, *Phys. Rev. B* **36**, 8565 (1987).
 - ¹⁹Gayanath W. Fernando and Bernard R. Cooper, *Phys. Rev. B* **38**, 3016 (1988).
 - ²⁰D. Bagayoko and J. Callaway, *Phys. Rev. B* **28**, 5419 (1983).
 - ²¹V. L. Moruzzi, *Phys. Rev. Lett.* **57**, 2211 (1986).
 - ²²Marek Podgórný, *J. Magn. Magn. Mater* **78**, 352 (1989).
 - ²³D. P. Pappas, C. R. Brundle, and H. Hopster, *Phys. Rev. B* **45**, 8169 (1992).
 - ²⁴D. Pescia, M. Stapanoni, G. L. Bona, A. Vaterlaus, R. F. Willis, and F. Meier, *Phys. Rev. Lett.* **58**, 2126 (1987).
 - ²⁵D. P. Pappas, K.-P. Kämper, B. P. Miller, H. Hopster, D. E. Fowler, A. C. Luntz, C. R. Brundle, and Z.-X. Shen, *J. Appl. Phys.* **69**, 5209 (1991).
 - ²⁶J. G. Tobin, G. D. Waddill, and D. P. Pappas, *Phys. Rev. Lett.* **68**, 3642 (1992).
 - ²⁷D. P. Pappas, K.-P. Kämper, and H. Hopster, *Phys. Rev. Lett.* **64**, 3179 (1990).
 - ²⁸R. F. Willis, J. A. C. Bland, and W. Schwarzacher, *J. Appl. Phys.* **63**, 4051 (1988).
 - ²⁹Pedro A. Montano, Gayanath W. Fernando, Bernard R. Cooper, E. R. Moog, H. M. Naik, S. D. Bader, Y. C. Lee, Y. N. Darci, H. Min, and J. Marcano, *Phys. Rev. Lett.* **59**, 1041 (1987).
 - ³⁰W. Becker, H.-D. Pfannes, and W. Keune, *J. Magn. Magn. Mater.* **35**, 53 (1983).
 - ³¹C. Liu, E. R. Moog, and S. D. Bader, *Phys. Rev. Lett.* **60**, 2422 (1988).
 - ³²R. Allenspach and A. Bischof, *Phys. Rev. Lett.* **69**, 3385 (1992).
 - ³³F. J. Himpsel and J. E. Ortega, *Phys. Rev. B* **46**, 9719 (1992).
 - ³⁴M. Grunze, G. Strasser, and O. Elshazly, *J. Vac. Sci. Technol. A* **4**, 2396 (1986).
 - ³⁵Th. Fauster, D. Straub, J. J. Donelon, D. Grimm, A. Marx, and F. J. Himpsel, *Rev. Sci. Instrum.* **56**, 1212 (1985).
 - ³⁶G. J. Mankey, M. T. Kief, and R. F. Willis, *J. Vac. Sci. Technol. A* **9**, 1595 (1991).
 - ³⁷N. V. Smith and L. F. Mattheiss, *Phys. Rev. B* **9**, 1341 (1974).
 - ³⁸R. Courths and S. Hüfner, *Phys. Rep.* **112**, 53 (1984).
 - ³⁹J. A. Knapp, F. J. Himpsel, and D. E. Eastman, *Phys. Rev. B* **19**, 4952 (1979).
 - ⁴⁰F. J. Himpsel, J. A. Knapp, and D. E. Eastman, *Phys. Rev. B* **19**, 2919 (1979).
 - ⁴¹W. Eberhardt and E. W. Plummer, *Phys. Rev. B* **21**, 3245 (1980).
 - ⁴²R. Schneider, K. Starke, K. Ertl, M. Donath, V. Dose, J. Braum, M. Grab, and G. Borstel (unpublished).
 - ⁴³A. Goldmann, M. Donath, W. Altmann, and V. Dose, *Phys. Rev. B* **32**, 837 (1985).
 - ⁴⁴K. Desinger, V. Dose, M. Göbl, and H. Scheidt, *Solid State Commun.* **49**, 479 (1984).
 - ⁴⁵R. Miranda, D. Chandris, and J. Lecante, *Surf. Sci.* **130**, 269 (1983).
 - ⁴⁶C. M. Schneider, J. J. de Miguel, P. Bressler, P. Schuster, R. Miranda, and J. Kirshner, *J. Electron Spectrosc. Relat. Phenom.* **51**, 263 (1990).
 - ⁴⁷C. M. Schneider, P. Schuster, M. Hammond, H. Ebert, J. Noffke, and J. Kirshner, *J. Phys. C* **3**, 4349 (1991).
 - ⁴⁸W. Clemens, T. Katchel, O. Rader, S. Blügel, C. Carbone, and W. Eberhardt, *Solid State Commun.* **81**, 739 (1992).
 - ⁴⁹A. Amiri Hezaveh, G. Jennings, D. Pescia, R. F. Willis, K. Prince, M. Surman, and A. Bradshaw, *Solid State Commun.* **57**, 329 (1986).
 - ⁵⁰M. F. Onellion, C. L. Fu, M. A. Thompson, J. L. Erskine, and A. J. Freeman, *Phys. Rev. B* **33**, 7322 (1986).
 - ⁵¹D. P. Pappas, K.-P. Kämper, B. P. Miller, H. Hopster, D. E. Fowler, C. R. Brundle, A. C. Luntz, and Z.-X. Shen, *Phys. Rev. Lett.* **66**, 504 (1991).
 - ⁵²H. Glatzel, R. Schneider, T. Fauster, and V. Dose, *Z. Phys. B* **88**, 53 (1992).
 - ⁵³A. Santoni and F. J. Himpsel, *Phys. Rev. B* **43**, 1305 (1991).
 - ⁵⁴P. Heimann, F. J. Himpsel, and D. E. Eastman, *Solid State Commun.* **39**, 219 (1981).
 - ⁵⁵H. I. Starnberg and P. O. Nilsson, *J. Phys. F* **18**, L247 (1988).
 - ⁵⁶J. E. Ortega and F. J. Himpsel, *Phys. Rev. Lett.* **69**, 844 (1992).
 - ⁵⁷F. J. Himpsel, *Phys. Rev. Lett.* **67**, 2363 (1991).
 - ⁵⁸I. Turek, Ch. Becker, and J. Hafner, *J. Phys. C* **4**, 7257 (1992).
 - ⁵⁹V. L. Moruzzi, J. F. Janak, and A. R. Williams, *Calculated Electronic Properties of Materials* (Pergamon, New York, 1978).